1268 *Biochemistry* **2010,** *49,* 1268–1280
DOI: 10.1021/bi901738k

BIOCHEMISTRY
including biophysical chemistry & molecular biology
*Article*

# Exploring the Roles of the Metal Ions in *Escherichia coli* Copper Amine Oxidase[†,‡]

Mark A. Smith,[§] Pascale Pirrat,[§] Arwen R. Pearson, Christian R. P. Kurtis, Chi H. Trinh, Thembaninkosi G. Gaule, Peter F. Knowles, Simon E. V. Phillips,[∥] and Michael J. McPherson*

*Astbury Centre for Structural Molecular Biology and Institute of Molecular and Cellular Biology, Faculty of Biological Sciences, University of Leeds, Leeds LS2 9JT, U.K.* [§]*M.A.S. and P.P. contributed equally to this work.* [∥]*Current address: Research Complex at Harwell (RCaH), Rutherford Appleton Laboratory, Harwell Science and Innovation Campus, Didcot OX11 0FA, U.K.*

*Received October 8, 2009; Revised Manuscript Received January 4, 2010*

ABSTRACT: To investigate the role of the active site copper in *Escherichia coli* copper amine oxidase (ECAO), we initiated a metal-substitution study. Copper reconstitution of ECAO (Cu-ECAO) restored only ~12% wild-type activity as measured by $k_{cat(amine)}$. Treatment with EDTA, to remove exogenous divalent metals, increased Cu-ECAO activity but reduced the activity of wild-type ECAO. Subsequent addition of calcium restored wild-type ECAO and further enhanced Cu-ECAO activities. Cobalt-reconstituted ECAO (Co-ECAO) showed lower but significant activity. These initial results are consistent with a direct electron transfer from TPQ to oxygen stabilized by the metal. If a Cu(I)-TPQ semiquinone mechanism operates, then an alternative outer-sphere electron transfer must also exist to account for the catalytic activity of Co-ECAO. The positive effect of calcium on ECAO activity led us to investigate the peripheral calcium binding sites of ECAO. Crystallographic analysis of wild-type ECAO structures, determined in the presence and absence of EDTA, confirmed that calcium is the normal ligand of these peripheral sites. The more solvent exposed calcium can be easily displaced by mono- and divalent cations with no effect on activity, whereas removal of the more buried calcium ion with EDTA resulted in a 60−90% reduction in ECAO activity and the presence of a lag phase, which could be overcome under oxygen saturation or by reoccupying the buried site with various divalent cations. Our studies indicate that binding of metal ions in the peripheral sites, while not essential, is important for maximal enzymatic activity in the mature enzyme.

Copper amine oxidases (CuAOs) catalyze the oxidative deamination of primary amines to the corresponding aldehydes, followed by the reduction of oxygen to hydrogen peroxide.

$$RCH_2NH_3^+ + O_2 + H_2O \rightarrow RCHO + NH_4^+ + H_2O_2$$

In bacteria CuAOs have a role in the utilization of primary amines as a source of nitrogen or carbon (*1*, *2*). In higher organisms, they are important in a variety of functions including cell adhesion and signaling (*3*−*8*). In humans three CuAOs have been identified, AOC1, also known as amiloride binding protein, AOC2, a retinal form, and AOC3, or vascular adhesion protein (VAP-1) (*9*). The most widely characterized of the three, VAP-1, is an endothelial transmembrane CuAO that mediates the interaction between lymphocytes and endothelial cells under inflammatory conditions facilitating transendothelial lymphocyte migration (*10*−*13*). CuAO production of formaldehyde has also been implicated in the alteration of protein structure, which may subsequently cause protein deposition associated with chronic vascular and neurobiological disorders, such as diabetic complications, atherosclerosis, and neurodegenerative disease (*7*, *14*). CuAOs are also implicated in adipose tissue regulation (*15*). Although the mechanisms underlying the various etiological outcomes are not fully understood, the development of highly selective amine oxidase inhibitors is underway (*16*).

The posttranslational modification of a conserved active site tyrosine in CuAO forms an organic cofactor, 2,4,5-trihydroxyphenylalanine quinone (TPQ)[1] (*17*, *18*). TPQ biogenesis is autocatalytic, requiring only copper and oxygen (*18*). Crystal structures of the *Escherichia coli* enzyme (ECAO) have provided a basis for detailed structure−function studies (*19*). ECAO is a homodimer of ~160 kDa (Figure 1), and the active site includes TPQ, stabilized in an "off-metal" conformation by interaction with Tyr369, and in this productive form of the enzyme the O5 of TPQ is positioned at the bottom of the substrate entry cleft close to the active site base Asp383. The cupric ion is coordinated by His524, His526, His689, and two water molecules, one equatorial and one axial.

The crystal structures of TPQ/copper amine oxidases from pea seedling (PSAO) (*20*), *Arthrobacter globiformis* (AGAO) (*21*), *Hansenula polymorpha* (HPAO) (*22*), *Pichia pastoris* lysyl oxidase (PPLO) (*23*), bovine serum amine oxidase (BSAO) (*24*), human vascular adhesion protein (VAP-1) (*25*), and human diamine oxidase (*26*) all display the same overall architecture and topology as ECAO, with the exception of the N-terminal domain which only exists in Gram-negative bacterial enzymes.

Since the early 1980s experiments have been carried out on a range of CuAOs to examine the role of the active site copper in activating molecular oxygen ($O_2$) and whether it is redox active

[†]This work was supported by the Biotechnology and Biological Sciences Research Council (Grant BB/C00468X/1) and by a Wellcome Trust Studentship (Grant 072570/Z/03/Z) to P.P. A.R.P. is an RCUK Academic Research Fellow.

[‡]File names for Brookhaven Protein Data Bank entries: $EDTA_1$, 2wof; $EDTA_2$, 2wo0; ECAO-$Sr^{2+}$, 2woh.

*Corresponding author. Tel: +44 (0)113 343 2595. Fax: +44 (0)113 343 2861. E-mail: m.j.mcpherson@leeds.ac.uk.

 Published on Web 01/07/2010 

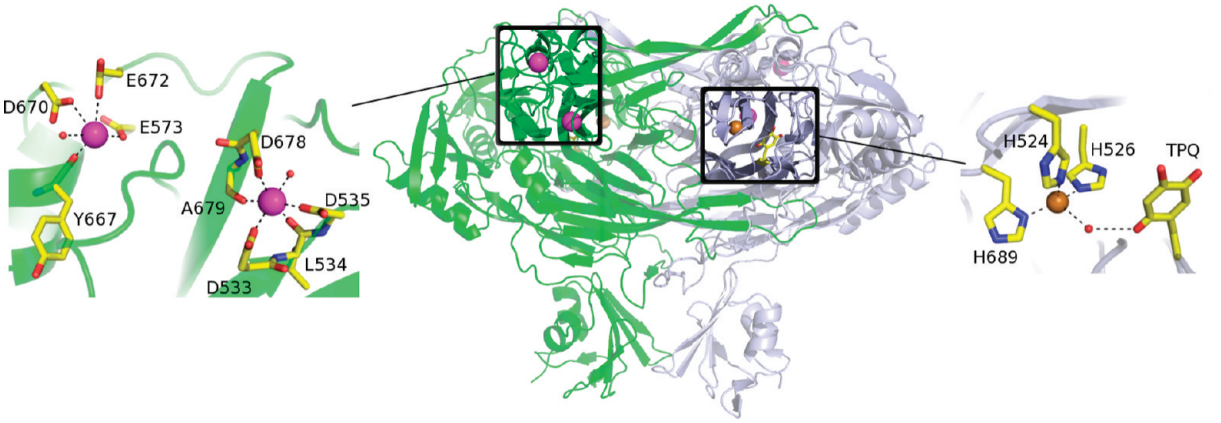


FIGURE 1: Structural overview of ECAO. In the center is a cartoon showing the ECAO dimer colored by monomer (1DYU). To the left is a more detailed view of the peripheral metal binding sites; to the right is a detailed view of the active site. Figure generated with Pymol (*73*).

during the oxidative half-cycle of catalysis (*27*−*37*). Two current models exist for the reoxidation of amine substrate reduced aminoquinol ($TPQ_{AMQ}$) to TPQ: (a) that copper plays an essential role in inner-sphere electron transfer from $TPQ_{AMQ}$ to $O_2$ by providing a binding site for reduced oxygen species, suggesting a potential redox-active role for copper (*33*) or (b) that electron transfer occurs by an outer-sphere mechanism whereby $TPQ_{AMQ}$ directly reduces dioxygen which is bound and activated in a hydrophobic pocket adjacent to the metal site, with no requirement for a change in the copper oxidation state (*34*). Recent experiments by Mukherjee et al. and Shepard et al. have provided further evidence for a redox role of copper in an inner-sphere electron transfer process (*38*, *39*) and are consistent with the existence of an on-pathway Cu(I)-TPQ semiquinone ($TPQ_{SQ}$) intermediate. However, as noted by Shepard et al., it seems increasingly likely that the precise reoxidation mechanism of $TPQ_{AMQ}$ in CuAOs is specific to the source of the CuAO (*39*).

While attention has focused naturally upon the roles of copper, TPQ, and various active site residues in CuAOs, the roles of the nonactive site metal ions, which lie at peripheral sites distant from the active site, have been largely ignored (Figure 1). In ECAO, there are two such peripheral metal ions, originally assigned as calcium from crystallographic data (*19*) and subsequently confirmed by inductively coupled plasma mass spectroscopy (ICP-MS) (*40*). These peripheral metal sites in ECAO lie close to the enzyme surface some 30 Å from the active site copper (Figure 1). One is in direct contact with solvent and will be referred to as the "surface site" while the other is not solvent exposed and will be referred to as the "buried site". The buried site is present in all CuAOs with the exception of HPAO, although HPAO contains an arginine (R467) in place of one of the buried site acidic ligands (Figure 2), raising the prospect that a salt bridge substitutes for the metal in this species. Interestingly, both peripheral metal sites are assigned as calcium in the mammalian CuAOs (though $Mn^{2+}$ has been reported in purified native human placental diamine oxidase (*41*)), and as calcium is a well-known regulatory metal, this may be of significance for their biological function. In contrast, two CuAOs from plant sources, PSAO (*20*) and fenugreek seedlings (*42*), are reported to contain $Mn^{2+}$ as their second site metal. $Mn^{2+}$ is highly abundant in plant seedlings, suggesting that metal availability is a possible determinant for the identity of the observed metal in these sites.

We initiated biochemical and kinetics studies to explore the effect of active site metal replacement in ECAO. One of the surprising outcomes of this work was to highlight the potential

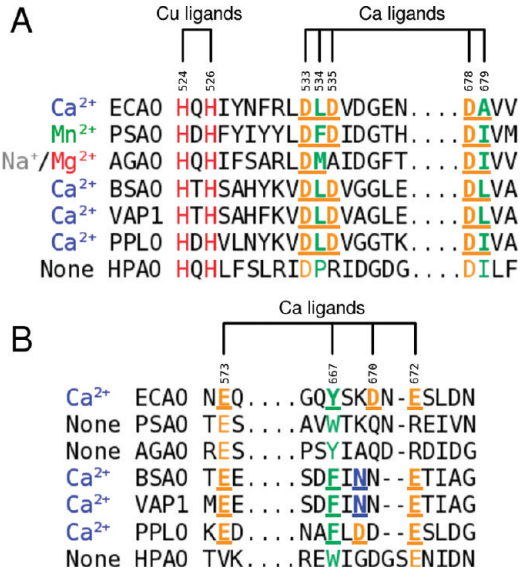


FIGURE 2: Amino acid alignment of seven copper amine oxidases in the regions of the peripheral metal sites. The alignment is based on a multiple sequence alignment (CLUSTALW (*74*)) including 30 CuAO from plants, animals, and bacteria and on the available crystal structures. (A) The buried site region is characterized by two $\beta$-strands that link the Cu(II) site via its ligands H524, H526, and H689 to the buried $Ca^{2+}$ site. (B) The surface site is less well conserved. Peripheral metal site ligands are indicated in bold and underlined. The copper ligands are shown in red, acidic peripheral site ligands in orange, and hydrophobic residues whose backbone carbonyls coordinate the peripheral sites in green. Asparagines in the surface site in BSAO and VAP1 are shown in blue. (ECAO, *Escherichia coli*; PSAO, pea seedling; AGAO, *Arthrobacter globiformis*, BSAO, bovine serum; VAP-1, human vascular adhesion protein; PPLO, *Pichia pastoris*; HPAO, *Hansenula polymorpha*.) ECAO numbering is used throughout, and the identity of the peripheral metal in each enzyme site is indicated.

importance of the peripheral calcium ions in ECAO. We have therefore examined the effects of EDTA treatment and of metal replacement at these sites on ECAO activity and three-dimensional structure.

## EXPERIMENTAL PROCEDURES

*Expression and Purification of ECAO*. ECAO protein was prepared from *E. coli* JM109 carrying recombinant plasmid pKKecao (*40*) essentially according to previously reported procedures (*40*, *43*) but with the following modifications.

A culture of *E. coli* JM109 carrying plasmid pKKecao (*40*) was grown in 2TY medium (500 mL) containing 50 $\mu$g/mL disodium carbenicillin, 25 $\mu$g/mL ampicillin, and 50 $\mu$M $CuSO_4$ at 37 °C with shaking (200 rpm) to $OD_{600}$ 0.6−0.8. Induction of ECAO expression was achieved by addition of 1 mM IPTG for 4−5 h. Cells were harvested for 10 min at 4 °C at 5000*g*, and all subsequent manipulations were carried out on ice. The cell pellet was resuspended in 10 mL of 50 mM Tris-HCl (pH 8.0) containing 20% sucrose. A 3 mL aliquot of 42 mM EDTA (pH 8.0) was added followed by a further 3 mL of 50 mM Tris-HCl (pH 8.0) containing 10 mg/mL lysozyme with intermittent agitation and incubated for 30 min. Six milliliters of 50 mM Tris-HCl (pH 8.0) containing 9% sucrose was then added followed by 13.5 mL of the same buffer containing 15 mM $MgCl_2$. The suspension was centrifuged at 10000*g* for 30 min to obtain the periplasmic fraction. The supernatant was dialyzed overnight against 20 mM Tris-HCl (pH 7.0) and loaded onto a Q-Sepharose ion-exchange column, previously equilibrated with 20 mM Tris-HCl (pH 7.0) and washed with 20 mM Tris-HCl (pH 7.0) followed by a second wash with 35 mM NaCl in 20 mM Tris-HCl (pH 7.0). A gradient from 35 to 175 mM NaCl in 20 mM Tris-HCl (pH 7.0) was then used to elute the protein. The purest fractions, identified by SDS−PAGE, were pooled and dialyzed versus 20 mM Tris-HCl (pH 7.0). ECAO was concentrated to 6−10 mg/mL, as estimated by $A_{280}$ measurement adjusted by a gravimetrically derived correction factor of 0.76 to give the concentration in milligrams per milliliter ($\varepsilon_{280} = 2.1 \times 10^5\ M^{-1}\ cm^{-1}$) (*44*). Pure ECAO was used directly for crystallization or flash frozen in liquid $N_2$ and stored at −80 °C.

*UV−Vis Spectroscopy*. UV−vis spectroscopic studies were performed on a Shimadzu UV2401 PC spectrophotometer equipped with a temperature-controlled cell holder at 25 ± 0.1 °C. TPQ content was determined by titration of the enzyme with 2-hydrazinopyridine (2-HP). In brief, 200 $\mu$L aliquots of ECAO (5 $\mu$M per monomer) in 100 mM sodium phosphate buffer (pH 7.0) were incubated with 0.1−1.0 mol equiv of the irreversible inhibitor 2-HP. Samples were incubated overnight; then spectra were recorded over the range 300−600 nm. The reaction was monitored by the formation of an initial adduct at ~430 nm and allowed to proceed until no further spectral change was detected following each addition (*45*).

*Activity Assays*. Enzyme activity was determined from the measurement of the initial rate of hydrogen peroxide production during the enzymatic oxidation of a primary amine substrate, using a coupled assay system (*19*). Briefly, the assay buffer contained 100 mM sodium phosphate buffer (pH 7.0), 2,2′-azinobis(3-ethylbenzthiazoline-6-sulfonoic acid) (ABTS) (0.3 mg/mL), horseradish peroxidase (0.1 mg/mL), and $\beta$-phenylethylamine at variable concentrations. To assess the effect of various treatments on the enzyme, specific activity was measured at a standard concentration of 10 $\mu$M $\beta$-phenylethylamine at which concentration ECAO activity equals $V_{max}$. Typically, to 980 $\mu$L assay buffer was added 20 $\mu$L of purified protein (0.2−0.05 $\mu$M; dimer of ECAO) and the reaction recorded at 410 nm in a Shimadzu 2401 UV−vis spectrophotometer. Steady-state kinetic parameters ($K_{M(amine)}$ and $k_{cat}$) were determined by changing the concentration of $\beta$-phenylethylamine (0.5−1000 $\mu$M) and calculated by fitting the data to nonlinear regression curves of the Michaelis−Menten equation using OriginPro. In addition, we determined the effect of oxygen on enzyme activity by comparing specific activity of the metal-reconstituted samples and wild-type enzyme under standard aerobic conditions and following oxygen purging of the assay solutions.

*Active Site Metal Replacement Studies*. All chemicals were purchased to the highest quality (≥99.99% pure). All work was carried out using plasticware which had been treated with 0.1 M EDTA (pH 7.3) (25 L bath prepared in $ddH_2O$ with resistivity ≥15 MΩ) for a minimum of 1 h at room temperature before rinsing with $ddH_2O$ (≥15 MΩ) and drying thoroughly. Buffers were prepared using Chelex-treated $H_2O$ (resistance ≥18.2 MΩ). All solutions were passed twice through a Chelex column (Chelex 100, 100−200 mesh sodium; Bio-Rad). No more than 5 L of buffer was passed through without regeneration of the Chelex matrix unless EDTA (≥1 mM) was added supplementary to Chelex treatment. The pH of the buffers was confirmed prior to work with ECAO. All solutions were degassed by purging with $N_2$ and with rigorous stirring for a minimum of 2−3 h (1 L of buffer in a plastic flask with minimum head space) before placing in an anaerobic cabinet (Belle Technology; ≤2 ppm $O_2$) overnight at ca. 25 °C. Sodium dithionite and KCN were placed in the cabinet overnight prior to addition to allow for equilibration. Analytical grade chloride salts of Co(II), Cu(II), Ni(II), and Zn(II) were purchased from Fisher Chemicals.

Attempts were made to substrate-reduce the wild-type ECAO with $\beta$-phenylethylamine as has been described for HPAO (*32*). However, yields of copper-free (Cu-free) ECAO were low using this method. Metal ions were therefore removed from wild-type ECAO using a modification of the method described previously for AGAO (*31*). Approximately 6 mL of 10 mg/mL wild-type ECAO was prepared and dialyzed aerobically overnight at 4 °C against 500 mL of Chelex-treated 50 mM HEPES (pH 6.8). The dialyzed protein was transferred to 500 mL of degassed, Chelex-treated 50 mM HEPES (pH 6.8) and equilibrated under anaerobic conditions in the Belle cabinet overnight at 25 °C. Solid sodium dithionite (50 mM) was added to a degassed solution of 50 mM HEPES (pH 6.8), and the protein was dialyzed for a minimum of 3 h during which it decolorized from strong to a very pale pink. Solid KCN was then added to 10 mM, and the dialysis continued overnight. The resulting metal-depleted ECAO was dialyzed extensively in 50 mM HEPES (pH 6.8) supplemented with 1 mM EDTA, followed by 50 mM HEPES (pH 6.8) alone.

The metal-depleted ECAO was then removed from the anaerobic cabinet, aliquoted into equal portions, and dialyzed versus Chelex-treated 50 mM HEPES (pH 6.8) supplemented with 1.4 mM $MCl_2$ ($M = Cu^{2+}, Ni^{2+}, Co^{2+}, Sr^{2+}, Zn^{2+}$) under aerobic conditions. All subsequent steps were performed under aerobic conditions. Following overnight dialysis at room temperature, the samples were removed, diluted by half with Chelex-treated 50 mM HEPES (pH 6.8), and further dialyzed versus non-Chelex-treated 20 mM Tris-HCl (pH 7.2) supplemented with 100 mM EDTA alongside a sample of wild-type ECAO. EDTA was removed by 4 h dialysis versus non-Chelex-treated 20 mM Tris-HCl (pH 7.2) alone. Samples were dialyzed overnight versus non-Chelex-treated 20 mM Tris-HCl (pH 7.2) supplemented with 1 mM $CaCl_2$. All samples were analyzed for metal content by ICP-MS and kinetic assays carried out.

*ECAO Sample Preparation for Solution Studies of Peripheral Metals*. Typically, wild-type ECAO was diluted in 20 mM Tris-HCl (pH 7.0), and the protein concentration was measured by $A_{280}$ (*44*). The sample was divided into aliquots, which were subjected to various treatments before measurement of enzyme activity. For EDTA treatment, a solution of EDTA was added to the enzyme to give a final concentration

of ≥1000-fold molar excess of EDTA to ECAO. The EDTA-treated ECAO samples were incubated at room temperature for at least 1 h before further additions or measurement of enzyme activity. The final concentration of EDTA in the assay mixture was reduced by dilution to ≤10 nM. At this concentration there was no effect of residual EDTA on either ECAO or the HRP used in the coupled assay. To remove EDTA from the enzyme solution, three to five buffer exchange steps against metal-free Chelex-treated 20 mM Tris-HCl buffer (pH 7.0) (see above) were performed using Microcon centrifugal filter devices (Amicon; 30 kDa MWCO) prior to metal addition.

*Metal Content Determination*. Samples of ECAO in aqueous solution were subjected to ICP-MS at the University of East Anglia using a Thermo Electron X7 ICP quadrupole mass spectrometer. An internal rhodium standard was used to correct for any instrument drift. Solvent standards were also analyzed.

*X-ray Crystallographic Data Collection*. ECAO crystals were grown by sitting drop vapor diffusion. Typically 5 μL of protein sample (6−10 mg/mL) was gently mixed with the same volume of mother liquor in a microbridge insert (Crystal Microsystems). Drops were equilibrated against mother liquor containing 100 mM HEPES (pH 6.9−7.2) and sodium citrate (1.10−1.35 M).

For EDTA-treated crystals ($EDTA_1$ and $EDTA_2$) 0.5 M EDTA in 20 mM Tris-HCl (pH 8.5) was added to an 8 mg/mL solution of wild-type ECAO to give a final concentration of 66 mM EDTA. After 4 h incubation, this enzyme solution was used to set up crystallization trays. For strontium treatment, wild-type (non-EDTA-treated) crystals grown as above were soaked for 50 h in 100 mM $SrCl_2$. ECAO crystals were recovered and incubated in cryoprotectant solution of crystal growth mother liquor containing 20% glycerol before being immediately flash frozen in liquid nitrogen for X-ray data collection. The collection of data for these crystals was performed both at SRS, Daresbury (Station 14.2; $EDTA_1$), and at ESRF, Grenoble (beamline BM14; $EDTA_2$).

The proteins crystallized in space group $P2_12_12_1$, as observed previously for ECAO (*19*), and contained a dimer in the asymmetric unit. Data were processed using MOSFLM (*46*) and SCALA (*47*). Further processing, model building, and refinement were carried out using the CCP4 suite (*48*). Details of crystal parameters, data collection, and refinement statistics are shown in Table 3.

*X-ray Crystallographic Structure Analysis*. The isomorphous wild-type ECAO structure 1DYU (*40*) was used as a starting model. All refinement and model building was performed using Refmac5 (*49*) and COOT (*50*), respectively. Rigid body refinement was used to optimize the orientation of the starting model. Then TPQ was replaced in each subunit by an alanine residue; all metal ions ($Cu^{2+}$ and $Ca^{2+}$) and all water molecules in the active site were deleted as were a number of other water molecules. After initial positional refinement COOT was used to build the missing side chains, to place the metals and water molecules where appropriate, and successive rounds of positional refinement and rebuilding generated the final model.

## RESULTS

*Active Site Metal Replacement. UV−Vis Spectroscopy and Kinetics*. The UV−vis spectral properties of the active site metal-reconstituted ECAOs are shown in Figure 3. The metal-depleted protein contained no detectable peak in the 450−500 nm region, suggesting the TPQ was in a reduced state. This spectrum remained essentially unchanged even after prolonged exposure to air-saturated buffer at room temperature (data not shown). The active site metal-reconstituted enzymes all contained a broad peak in the 450−550 nm range with all measurements being made at pH 7.0.

Metal determination by ICP-MS (Table 1) indicates that Cu substitution is almost complete at 0.95 atom/subunit with Ni substitution at 0.82 atom/subunit and the Co-substituted substantially lower at only ∼0.5 atom/subunit. Kinetic analyses allowed determination of $K_{M(amine)}$ and $k_{cat}$ and for the EDTA-treated samples and subsequent calcium-treated samples. These data were corrected for metal content and are shown in Table 2. For the initial Cu-, Ni-, and Co-reconstituted samples the $K_{M(amine)}$ was similar to wild type, but $k_{cat}$ was reduced, resulting in $k_{cat}/K_{M(amine)}$ values of 1.25, 0.004, and 0.25 $\mu M^{-1}$ $s^{-1}$ corresponding to 12.1%, 0.39%, and 2.4%, respectively, compared with the wild-type untreated ECAO. It should be noted that the metal-depleted enzyme showed ca. 1% wild-type activity. The Zn-substituted ECAO was inactive in the assay and thus below the level of detectable activity of $k_{cat}$ $1.2 \times 10^{-5}$ $s^{-1}$ (*40*).

As shown in Table 1, the dialysis step with the replacement metals resulted in samples containing excess metal ions, which may account for the lower than expected levels of enzyme activity (Table 2 and Figure 4). To overcome any potential inhibitory effects of exogenous metal ions, samples were further dialyzed versus 100 mM EDTA. This treatment had an adverse effect on the activity of the wild-type ECAO, resulting in a $k_{cat}/K_{M(amine)}$ of 6.08 $\mu M^{-1}$ $s^{-1}$, which represents a 49% reduction compared with untreated ECAO. As anticipated, however, the EDTA treatment resulted in the $k_{cat}/K_{M(amine)}$ values for Cu-ECAO, Ni-ECAO, and Co-ECAO increasing to 4.21, 0.1, and 0.86 $\mu M^{-1}$ $s^{-1}$, which represent 69%, 1.7%, and 14%, respectively, compared with the EDTA-treated wild-type value. For all of these forms of metal-reconstituted ECAO the $\lambda_{max}$ values were 485 ± 2 nm (Figure 3A) with metal content corrected molar extinction coefficients of 1726, 2210, and 2750 $M^{-1}$ $cm^{-1}$ for Cu-, Ni-, and Co-ECAO, respectively.

The unexpected reduction in activity of the EDTA-treated wild-type ECAO led to the proposal that calcium bound in the peripheral metal sites may be removed from the enzyme during this treatment, resulting in reduced activity. It was also observed, during initial evaluation of the catalytic function of the metal-replaced enzyme, that the initial rate of amine oxidation increased over time. As the assay buffer had not been Chelex treated, it was concluded that trace amounts of a divalent metal ion might be responsible.

Table 1: ICP-MS Analysis of Metal Content (Indicated in Parentheses) for Metal Removal and Replacement and Subsequent Treatments

| ECAO | metal content (mol of atom/mol of subunit) |
|---|---|
| wild type | 1.05 ± 0.01 (Cu) |
| apo (Cu-free) | 0.009 ± 0.0002 (Cu) |
| Cu-replaced (Cu-ECAO) | 8 ± 0.05 (Cu) |
| Ni-substituted (Ni-ECAO) | 10 ± 0.2 (Ni) |
| Co-substituted (Co-ECAO) | 11 ± 0.1 (Co) |
| Cu-ECAO (+EDTA) | 0.95 ± 0.01 (Cu) |
| Ni-ECAO (+EDTA) | 0.81 ± 0.02 (Ni) |
| Co-ECAO (+EDTA) | 0.5 ± 0.02 (Co) |
| Cu-ECAO (+calcium) | 0.92 ± 0.01 (Cu) |
| Ni-ECAO (+calcium) | 0.82 ± 0.02 (Ni) |
| Co-ECAO (+calcium) | 0.49 ± 0.02 (Co) |

To explore this further, the EDTA-treated metal-reconstituted enzyme samples were dialyzed against 1 mM $CaCl_2$. There was little change in the active site metal contents (Table 1), and the level of copper present in the Ni-ECAO and Co-ECAO samples after calcium addition was maximally 1% and 2%, respectively. The wild-type enzyme activity was restored to a $k_{cat}/K_{M(amine)}$ of 10.83 $\mu M^{-1}$ $s^{-1}$ while the Cu-ECAO and Co-ECAO also showed increases in $k_{cat}/K_{M(amine)}$ to 7.07 and 0.4 $\mu M^{-1}$ $s^{-1}$, representing 65% and 4% of the activity of the restored wild-type value. In contrast, the Ni-ECAO activity decreased to a $k_{cat}/K_{M(amine)}$ value of 0.05 $\mu M^{-1}$ $s^{-1}$ or only 0.5% of the restored wild-type activity. The addition of $Ca^{2+}$ to the Cu-ECAO, Ni-ECAO, and Co-ECAO resulted in shifts in the $\lambda_{max}$ values to 471, 493, and 462 nm, respectively (Figure 3B), and with corrected extinction coefficients of 2891, 2561, and 2612 $M^{-1}$ $cm^{-1}$, respectively. The changes in $\lambda_{max}$ presumably reflect differences in the active site environment in these three enzyme forms, but this was not investigated further in this study.

Experiments were also carried out to investigate the possibility that oxygen binding was altered in metal-substituted ECAOs in accordance with the observations of Mills et al. in HPAO (*34*). Under saturating oxygen conditions no change in activity was observed for the Cu-ECAO or Ni-ECAO. However, the Co-ECAO did show a modest increase compared with air-saturated conditions in both $k_{cat}$ (0.27−0.43 $s^{-1}$) and $K_{M(amine)}$ (0.6−0.68 $\mu M$), resulting in a $k_{cat}/K_{M(amine)}$ increase from 0.44 to 0.63 $\mu M^{-1}$ $s^{-1}$. This is a very modest increase compared with that reported for the Co-HPAO which under saturating oxygen

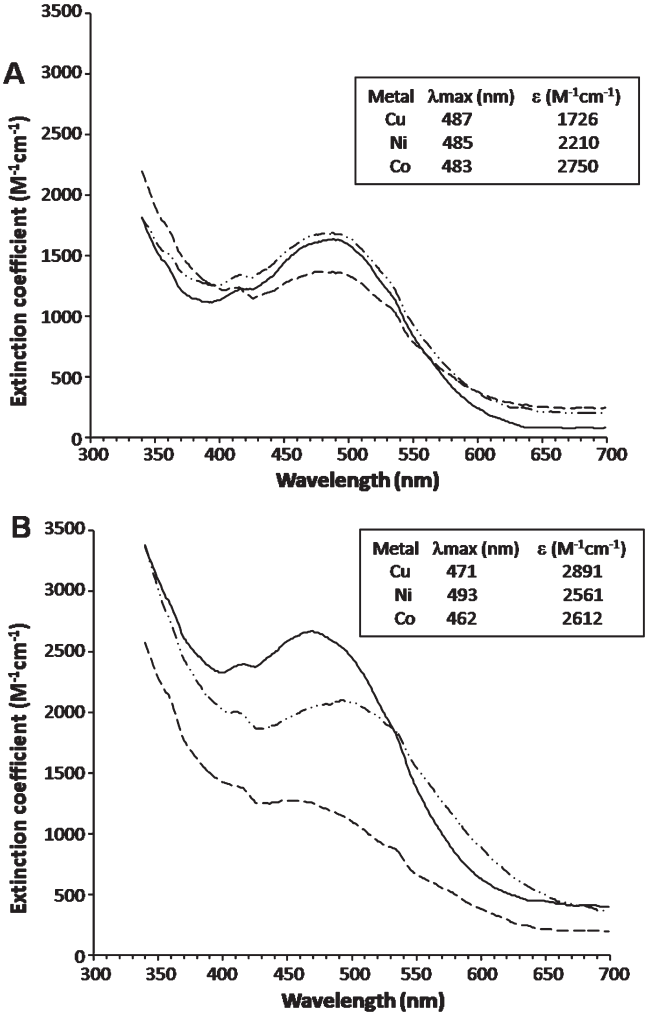


FIGURE 3: UV−vis spectra of metal-reconstituted ECAO. (A) Post EDTA treatment. (B) Following addition of calcium. Solid line, Cu-ECAO; dot-dashed line, Ni-ECAO; dashed line, Co-ECAO. The $\lambda_{max}$ and extinction coefficient ($M^{-1}$ $cm^{-1}$) values corrected for metal content are shown in the insert tables.

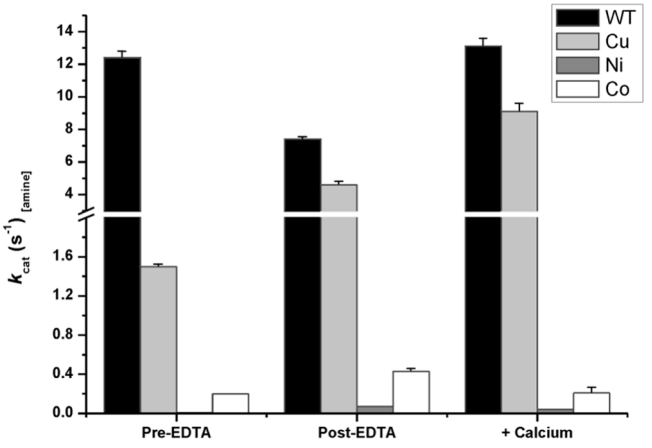


FIGURE 4: ECAO turnover ($k_{cat}$) profile of the active site metal replacement studies.

Table 2: Kinetic Parameters for ECAO during Active Site Metal Reconstitution[a]

| enzyme | $k_{cat}$ ($s^{-1}$) | $K_M$ ($\mu M$) | $k_{cat}/K_M$ ($\mu M^{-1}$ $s^{-1}$) | relative activity |
|---|---|---|---|---|
| wild-type ECAO untreated | 12.4.0 ± 0.6 | 1.2 ± 0.1 | 10.33 | 100 |
| copper-reconstituted (Cu-ECAO) | 1.5 ± 0.025 | 1.2 ± 0.2 | 1.25 | 12.1 |
| nickel-reconstituted (Ni-ECAO) | 0.01 ± 0.001 | 1.46 ± 0.2 | 0.004 | 0.39 |
| cobalt-reconstituted (Co-ECAO) | 0.2 ± 0.006 | 0.8 ± 0.15 | 0.25 | 2.4 |
| wild-type EDTA-treated | 7.3 ± 0.4 | 1.2 ± 0.15 | 6.08 | 100 |
| Cu-ECAO EDTA-treated | 4.84 ± 0.16 | 1.15 ± 0.19 | 4.21 | 69 |
| Ni-ECAO EDTA-treated | 0.09 ± 0.004 | 0.9 ± 0.2 | 0.1 | 1.7 |
| Co-ECAO EDTA-treated | 0.86 ± 0.06 | 1.0 ± 0.3 | 0.86 | 14 |
| wild-type calcium-treated | 13.0 ± 0.6 | 1.2 ± 0.3 | 10.83 | 100 |
| Cu-ECAO calcium-treated | 9.89 ± 0.6 | 1.4 ± 0.4 | 7.07 | 65 |
| Ni-ECAO calcium-treated | 0.05 ± 0.002 | 1.0 ± 0.2 | 0.05 | 0.5 |
| Co-ECAO calcium-treated | 0.27 ± 0.08 | 0.6 ± 0.1 | 0.44 | 4 |
| Co-ECAO calcium-treated $O_2$ satd | 0.43 ± 0.1 | 0.68 ± 0.1 | 0.63 | 5.8 |

[a]Dithionite-reduced and cyanide metal-depleted enzyme was prepared and reconstituted and subsequently treated with EDTA and addition of calcium. Values for $k_{cat}$ and $k_{cat}/K_{M(amine)}$ are corrected for the variable metal content (Table 1) in the reconstituted enzymes. The relative activities are given as a percentage of the corresponding wild-type treated enzyme.

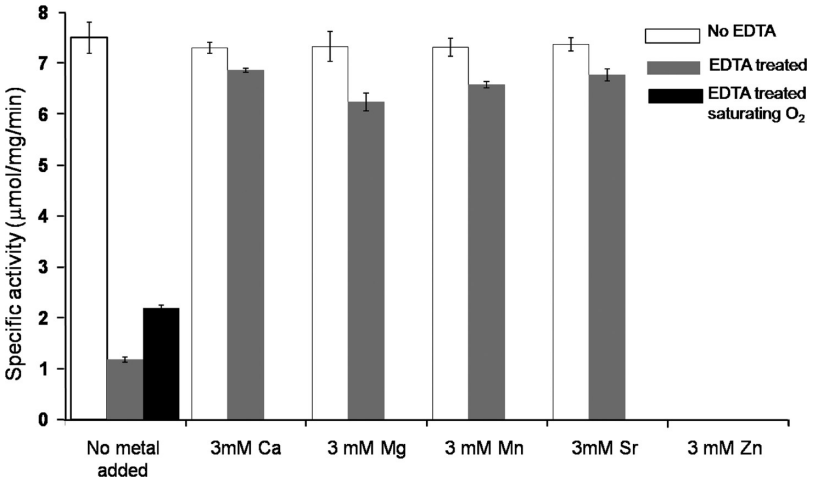


FIGURE 5: Activity profile of ECAO, with and without EDTA treatment, showing the effects of supplementation with additional metals ($Ca^{2+}$, $Mn^{2+}$, $Mg^{2+}$, $Sr^{2+}$, $Zn^{2+}$).

conditions exhibited a $k_{cat}$ identical to that of the wild-type enzyme (*32*).

These initial results of active site metal replacement studies suggested that, in ECAO, copper is the most efficient catalytic metal with cobalt displaying ca. 5.8% wild-type activity in terms of $k_{cat}/K_{M(amine)}$ under oxygen saturation. It is clear, however, that other divalent cations, specifically $Ca^{2+}$, associated with peripheral binding sites on the enzyme, influence the active site of the enzyme, a phenomenon that we went on to investigate further.

*Roles of Peripheral Metal Sites. Solution Studies.* To examine the role of the non active site calcium ions in ECAO, we used EDTA to effect their removal from wild-type ECAO. EDTA can chelate, with different stability constants (log $K_1$) (*51*), various divalent metal ions including calcium ($Ca^{2+}$; 10.70), manganese ($Mn^{2+}$; 13.56), magnesium ($Mg^{2+}$; 8.69), and strontium ($Sr^{2+}$; 8.63), with a strong preference for zinc ($Zn^{2+}$; 16.5) and copper ($Cu^{2+}$; 18.8). Although ECAO is a copper-containing enzyme, previous studies on CuAOs have shown that the deeply buried active site copper is tightly bound and is not accessible to EDTA (*29*, *52*, *53*). However, it was anticipated that the positions of the calcium ions close to the surface of ECAO would facilitate their removal by EDTA.

EDTA treatment at a final concentration of 1 mM (EDTA: $ECAO_{dimer}$ = 5000:1) caused a consistent reduction (60−90%) in enzyme activity with an associated lag of up to 4 min in attaining maximal activity with $\beta$-phenylethylamine. The addition of $Mg^{2+}$, $Mn^{2+}$, $Ca^{2+}$, or $Sr^{2+}$ to EDTA-treated enzyme, to a final concentration of 3 mM, prevented the lag phase and led to a good recovery of activity (Figure 5). When these metals were added directly to buffers containing untreated ECAO, the activities remained unchanged (Figure 5). Activity measurements on the EDTA-treated enzyme under saturating oxygen also reduced the lag phase and resulted in ca. 2-fold higher specific activity (Figure 5). There was no effect of oxygen concentration on the activity of any of the other enzyme samples. The addition of excess zinc abolished ECAO activity, and it is possible this is due to binding in the region of the active site base, forcing TPQ into a nonproductive conformation (*54*, *55*).

*Crystallographic Studies. Effect of EDTA Treatment.* The solution data suggested that the reduction in enzyme activity observed upon EDTA treatment was due to the removal of calcium ions from their binding sites. We therefore determined the structure of ECAO from crystals grown in the presence of EDTA ($EDTA_1$; PDB code 2wof) or soaked in strontium (strontium complex; PDB code 2woh). A second EDTA-treated ECAO data set ($EDTA_2$; PDB code 2wo0) was collected at an X-ray wavelength of 1.77 Å to maximize any anomalous signal from copper or calcium. In addition, a non-EDTA-treated wild-type ECAO data set recorded at an X-ray wavelength of 1.48 Å was also analyzed (*56*). These various structures were compared with previously determined structures of wild-type ECAO 1DYU, grown in sodium citrate (*40*), and 1OAC, grown in ammonium sulfate (*19*). Crystallographic data collection and refinement statistics are summarized in Table 3.

The EDTA-treated structures were resolved to 2.25 Å ($EDTA_1$) and 2.6 Å ($EDTA_2$) and showed essentially no difference in overall structure compared with structures of the untreated enzyme (1DYU). However, there was a difference in TPQ conformation within the active site. In 1DYU the TPQ is exclusively in a productive off-copper conformation (Figure 1) in which O5 is positioned for attack by the incoming amine substrate and subsequent catalysis. By contrast, in the EDTA-treated structure $EDTA_1$, after the first round of positional refinement the density for TPQ, modeled as alanine at this stage, was clear and corresponded to a mixture of the two previously reported conformers, on-copper and off-copper (Figure 6A). After several well-defined water molecules were added and a further five cycles of refinement performed, TPQ was rebuilt with occupancy of 0.5 for each conformation and refined with a final *B*-factor of around 25 $Å^2$ for each. The *B*-factors for copper were of similar value and the $F_{o(EDTA_1)} - F_{c(1DYU)}$ map did not display any negative peaks, indicating that the copper site was fully loaded and had not been affected by the EDTA treatment.

Differences were also observed upon examination of the electron density difference $F_{o(EDTA_1)} - F_{c(1DYU)}$ map in the region of the peripheral metal sites which showed a negative peak of 7 rms on the buried metal site but, surprisingly, no negative peak at the surface metal site (Figure 6B). This suggested that in the EDTA-treated crystals the calcium ions were missing from the buried site but were apparently still present in the surface site. However, when both calcium ions were removed from the 1DYU model, followed by 20 cycles of restrained refinement of this calcium-free model, a strong positive peak was observed at both sites in the $F_o - F_c$ map, suggesting that metal ions were present in both sites.

Table 3: Crystallographic Statistics for Data Collection and Structure Refinement

| data set | $EDTA_1$ | $EDTA_2$ | strontium complex |
|---|---|---|---|
| X-ray source | SRS | ESRF | home source |
| | 14.2 | BM14 | Rigaku RU-200 |
| X-ray detector | Quantum 4 ADSC CCD | MAR225 CCD detector | R-axis IV++ |
| X-ray wavelength (Å) | 0.98 | 1.77 | 1.54 |
| temperature (K) | 100 | 100 | 100 |
| space group | $P2_12_12_1$ | $P2_12_12_1$ | $P2_12_12_1$ |
| unit cell *a*, *b*, *c* (Å) | 135.1, 166.9, 79.8 | 134.7, 166.6, 79.8 | 135.1, 166.9, 79.8 |
| resolution (Å) | 51.3−2.25 (2.37−2.25) | 49.0−2.6 (2.74−2.60) | 39.6−2.7 (2.85−2.70) |
| no. of unique reflections | 86158 (12459) | 56001 (8057) | 49169 (7228) |
| multiplicity | 4.4 (4.5) | 3.6 (3.6) | 3.1 (3.0) |
| Wilson *B*-factor | 31.4 | 48.8 | 59.9 |
| completeness (%) | 99.9 (100.0) | 99.9 (99.8) | 98.1 (99.5) |
| $\langle I/\sigma \rangle$ (final shell) | 13.7 (3.9) | 13.2 (3.9) | 14.3 (3.6) |
| $R_{merge}$ (%)[a] | 9.1 (40.8) | 7.3 (23.7) | 7.2 (30.2) |
| $R_{factor}$ (%)[b] | 16.9 (22.9) | 18.2 (28.8) | 18.6 (28.6) |
| $R_{free}$ (%)[c] | 22.0 (29.1) | 24.8 (39.2) | 24.3 (41.0) |
| no. of reflections | 83024 (6007) | 54013 (4072) | 46643 (3457) |
| no. of reflections, $R_{factor}$ set | 80077 (5786) | 52095 (3914) | 44149 (3279) |
| no. of reflections, $R_{free}$ set | 2947 (221) | 1918 (158) | 2494 (178) |
| no. of non-hydrogen atoms | 12678 | 11794 | 11969 |
| no. of of protein atoms | 11402 | 11386 | 11366 |
| no. of ligand atoms | 6 | 6 | 6 |
| no. of solvent atoms | 1060 | 400 | 597 |
| average *B* (Å$^2$) | | | |
| overall | 35.7 | 29.7 | 40.5 |
| main chain | 34.2 | 29.2 | 40.3 |
| side chain | 35.8 | 29.9 | 40.4 |
| ligands | 33.8 | 33.8 | 44.3 |
| solvent | 43.2 | 34.2 | 43.3 |
| rmsd from ideality | | | |
| bonds (Å) | 0.02 | 0.01 | 0.004 |
| angles (deg) | 1.70 | 1.60 | 0.853 |
| Ramachandran plot | | | |
| most favored (%) | 97.8 | 95.9 | 97.5 |
| allowed regions (%) | 2.2 | 3.9 | 2.5 |
| disallowed regions (%) | 0 | 0.2 | 0.1 |
| PDB code | 2wof | 2wo0 | 2woh |

[a] $R_{merge} = \sum_h \sum_l |I_{hl} - \langle I_h \rangle| / \sum_h \sum_l \langle I_h \rangle$, where $I_{hl}$ is the *l*th observation of reflection *h*. [b] $R_{factor} = \sum||F_o| - |F_c|| / \sum|F_o|$, where $|F_o|$ is the observed structure factor amplitude and $|F_c|$ is the calculated structure factor amplitude. [c] $R_{free}$ is the *R* factor calculated for only the data excluded from refinement.

To clarify this apparent contradiction, both calcium ions were reintroduced into the $EDTA_1$ model at full occupancy with *B*-factor values from the 1DYU starting model (*B*-factor of surface sites $Ca^{2+}$ = 54.28 and 51.85 and buried sites $Ca^{2+}$ = 23.61 and 25.77, chains A and B, respectively). After positional and *B*-factor refinement, there was essentially no change in the *B*-factors of the calcium in the surface metal site when compared to the starting model. Interestingly, as observed in the 1DYU structure, the surface metal *B*-factors were considerably higher than those of the surrounding protein ligands, suggesting that the $Ca^{2+}$ occupancy at this site is less than 1 in both $EDTA_1$ and 1DYU. In contrast, the *B*-factors of the buried metal doubled, suggesting that occupancy of the buried site is substantially reduced by EDTA. The occupancy of the calcium at the buried site was therefore refined, and with 60% calcium occupancy, the *B*-factors of this metal ion were refined to similar values to its protein ligands, ~25 Å$^2$. Similar observations were made following analysis of an independent EDTA-treated ECAO crystal (data not shown).

These results could suggest that both sites remained partially occupied by calcium after EDTA treatment. However, an alternate, and more likely, explanation would be that these sites actually contain a smaller cation at full occupancy. In order to confirm the identity of the ion in these sites after EDTA treatment, data were collected from a crystal of EDTA-treated ECAO at 1.77 Å where calcium has a detectable anomalous signal ($EDTA_2$, $f''_{Ca}$ = 1.64, $f''_{Cu}$ = 0.76). The resulting anomalous difference map showed a clear 4 rms peak at each copper site but no peak at the buried or surface sites, indicating no calcium was present in either site. These data indicate that EDTA treatment is able to successfully remove calcium from both the surface and buried sites and that the observed electron density at this position must be due to a different ion with no anomalous signal at 1.77 Å. As the crystals were grown in high concentrations of sodium citrate (1.2 M), we modeled sodium ions ($f''_{Na}$ = 0.16) into both sites at full occupancy. After refinement both peripheral metal ions had similar *B*-factors to their protein ligands, and the $F_{o(EDTA_1)} - F_{c(EDTA_1)}$ electron density map no longer showed strong difference features, indicating sodium is likely to be bound in both sites.

Interestingly, our reexamination of the 1DYU structure, which was also grown in 1.2 M sodium citrate, called into question the identity of the surface metal ion in this structure. Unfortunately, the 1DYU data were collected at 0.99 Å where there is little detectable calcium anomalous signal ($f''_{Ca}$ = 0.58). We therefore calculated an anomalous difference map from another available data set representative of the non-EDTA-treated wild type,

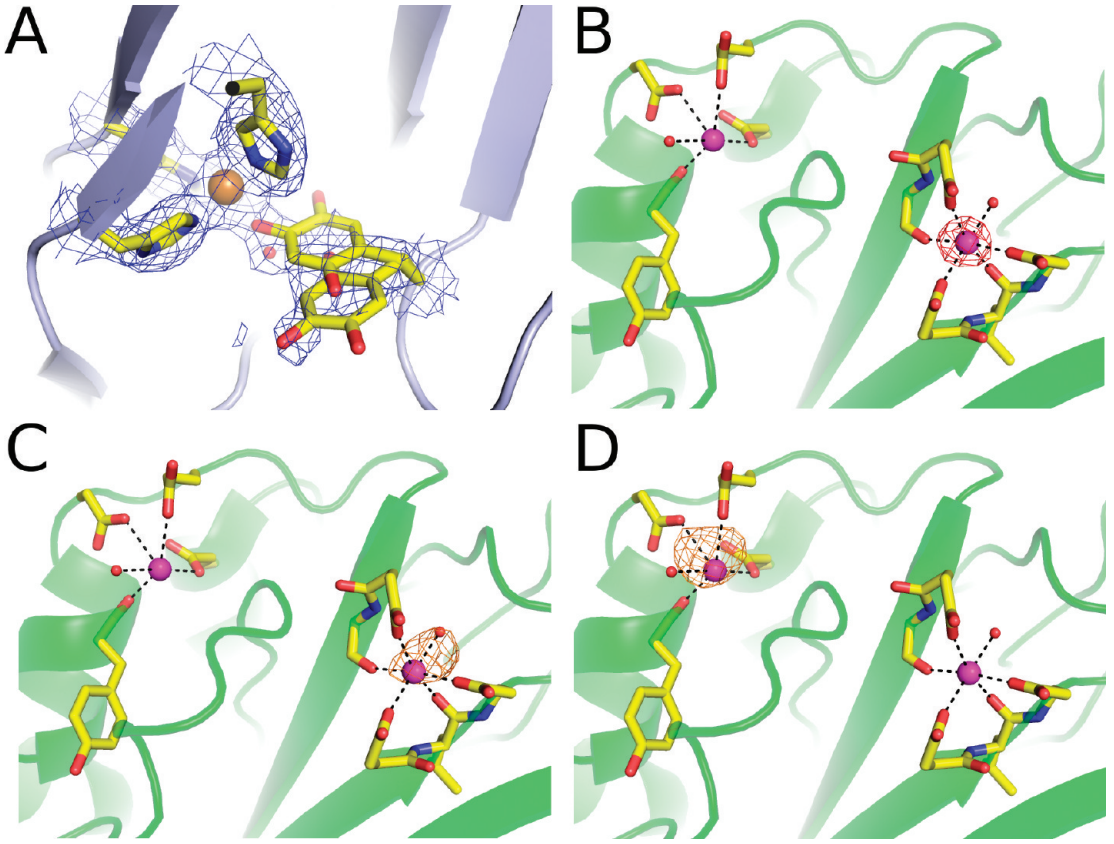


FIGURE 6: Crystallographic studies identifying the nature of the peripheral metal ions. (A) Detail of the active site in EDTA-treated ECAO showing the multiple conformations of TPQ. $2F_o - F_c$ density is shown as a blue mesh contoured at 1 rms. (B) A strong negative peak is observed at the site of the buried calcium in an $F_{o(EDTA)} - F_{o(1DYU)}$ map contoured at $-5\sigma$ and shown as red mesh. No difference peak is observed at the surface site. (C) A strong positive peak is observed at the buried site in an anomalous difference map calculated from an ECAO data set collected at 1.48 Å, indicating that this site is likely occupied by calcium in the absence of EDTA treatment. Positive anomalous difference density is shown as an orange mesh contoured at $4\sigma$. (D) A strong positive feature is observed at the surface site in the $Sr^{2+}$ complex structure in an $F_{o(Sr)} - F_{o(1DYU)}$ difference map. No peak is observed at the buried site, indicating strontium has only displaced the surface metal ion. The difference density is shown as an orange mesh contoured at $8\sigma$. Figure generated with Pymol (*73*).

a xenon derivative of ECAO (ECAO-Xe) (*56*). This data set was collected at 1.48 Å where calcium does have a detectable anomalous signal ($f''_{Ca} = 1.19$).

A strong anomalous peak (8.5 and 8 rms in subunits A and B, respectively) was found in the buried calcium site for the xenon derivative data, as well as a weaker but significant peak at the copper site ($f''_{Cu} = 0.54$). However, no anomalous signal could be detected at the surface site in either subunit (Figure 6C). These results indicate that the surface site in the xenon derivative ECAO structure, which has not been treated with EDTA, is not occupied by $Ca^{2+}$ but by a metal ion with no anomalous signal at 1.48 Å. This metal ion is not removed by EDTA, as there was no difference in site occupancy following EDTA treatment. The obvious candidate was $Na^+$, since the mother liquor in which the crystal grew contained 1.2 M sodium citrate, and $Na^+$ has negligible anomalous signal at these wavelengths (1.48 Å, $f''_{Na} = 0.11$, and 1.77 Å, $f''_{Na} = 0.16$). As the 1DYU crystal was also grown in sodium citrate, we rerefined this structure (*40*), replacing the surface site calcium with a sodium ion. In this rerefined 1DYU model, the *B*-factors for the surface metal sites decreased to values similar to those of the protein ligands, strongly suggesting that in crystals grown in 1.2 M sodium citrate sodium ions are likely to occupy the surface sites irrespective of whether the sample has been treated with EDTA.

In contrast, in the very first ECAO structure determined (1OAC (*19*)), for which the crystal was grown in 2.3 M ammonium sulfate, both peripheral metals were assigned as calcium. In this structure the *B*-factors of the metals and ligands are similar, suggesting that, in this case, the assignment of the surface metal ion as calcium is correct. This is supported by the conformation of D670, a surface site ligand, which in 1OAC is coordinated to the metal ion, consistent with the presence of a divalent cation. In contrast, in structures determined from crystals grown in sodium citrate a strong negative peak is observed on the D670 side chain in $F_{o(1DYU)} - F_{c(1OAC)}$, $F_{o(EDTA_1)} - F_{c(1OAC)}$, and $F_{o(ECAO\text{-}Xe)} - F_{c(1OAC)}$ difference maps, indicating that D670 is no longer a ligand in these structures. This is consistent with the presence of a monovalent metal ion such as $Na^+$. As final confirmation of the ability of a buffer metal ion to displace calcium in the surface site, we collected X-ray diffraction data from a crystal of non-EDTA-treated ECAO grown in 1.2 M sodium citrate and soaked with 100 mM strontium chloride (Table 3). In this structure, strontium could be modeled at full occupancy in the surface site of both subunits, with D670 as a ligand, but no strontium was detectable in the buried sites (Figure 6D). These data indicate that strontium displaces sodium from the surface site, suggesting a preference for divalent metal ions in this site. However, strontium is unable to displace calcium from the buried site.

## DISCUSSION

*Active Site Metal.* Cu-free ECAO remains colorless and is resistant to oxidation, confirming the successful removal of copper ion and confirming that no contaminating metals were

able to enter the active site and reoxidize the TPQ cofactor. Reconstitution with $Cu^{2+}$, or substitution with $Co^{2+}$, $Ni^{2+}$, or $Zn^{2+}$ resulted in reoxidation and recolorization of the TPQ cofactor, with recovery of 12.1% wild-type ECAO activity when copper was added. Although both Ni-ECAO and Co-ECAO support amine oxidation, their respective catalytic efficiencies are poor: 0.39% and 2.4%, respectively, compared with wild-type ECAO. To put these values into context, the background level of activity associated with the metal-depleted enzyme was ca. 1% of wild-type activity. Zinc was found to completely inactivate ECAO.

As copper reconstitution did not restore a high level of ECAO activity, we hypothesized that excess metal ions have an inhibitory effect. To remove any excess metal, the Cu-ECAO, Ni-ECAO, and Co-ECAO were treated with EDTA. Surprisingly, wild-type ECAO treated with EDTA showed a 49% reduction in activity. In contrast, EDTA treatment resulted in a substantial increase in the Cu-ECAO activity to 69% that of the EDTA-treated wild-type ECAO. The Co-ECAO and Ni-ECAO showed more modest levels of recovery of activity to 14% and 1.7% of the wild type. The unexpected reduction in activity of the wild type led to the suggestion that EDTA treatment of wild-type ECAO had removed the peripheral calcium ions. In order to test whether this was the case, we added excess calcium to both EDTA-treated wild-type ECAO and EDTA-treated metal-reconstituted ECAO. This resulted in the restoration of full activity to the wild-type ECAO and a further substantial increase in activity of Cu-ECAO to 65% that of fully active wild-type ECAO. The activity of Ni-ECAO decreased and is essentially indistinguishable from metal-depleted enzyme. There was also a reduction in Co-ECAO activity upon addition of calcium, although the activity was still ca. 4% of wild type. Previous studies with Co-HPAO showed a similar reduction in activity due to a substantial increase in the $K_M$ for oxygen such that under oxygen saturating conditions the Co-HPAO displayed the same turnover rate as wild-type enzyme (*32*). To examine whether there was an effect of oxygen concentration on ECAO, we compared $k_{cat}$ and $K_{M(amine)}$ under air-saturated and oxygen-saturated conditions. For Cu-ECAO and Ni-ECAO there was no effect, while for Co-ECAO we observed a modest increase in $k_{cat}$ from 0.27 to 0.43 $s^{-1}$; however, this is significantly different from the value of 9.8 $s^{-1}$ for Cu-ECAO, and so Co-ECAO does not show the same substantial level of recovery of activity as does Co-HPAO under oxygen saturation (*32*). Another example of appreciable activity in a Co-substituted enzyme was presented for bovine serum amine oxidase (BSAO) by Suzuki et al. (*27*), who reported 13.3% of native BSAO activity which corrects to 18.2% when allowance is made for the 73% Co content.

A red shift of the $\lambda_{max}$ for TPQ to ca. 485 nm (cf. wild-type ECAO $\lambda_{max}$ of 477 nm) was observed for all metal-substituted ECAOs upon EDTA treatment. After calcium addition, the $\lambda_{max}$ values of the TPQ cofactor in all metal-substituted ECAOs varied considerably (Co-ECAO, 462 nm; Cu-ECAO, 471 nm; Ni-ECAO, 493 nm). The $\lambda_{max}$ shifts are indicative of changes in the TPQ environment, suggesting differences in TPQ mobility in the different ECAO forms (*40*, *57*). This suggests that the treatment with EDTA affects the active sites in all the enzyme forms in a similar manner, perhaps resulting in a constraint on the TPQ configuration. Upon addition of calcium the active site environment must change, reflected by the divergence in the TPQ spectral feature.

Moving now to $Zn^{2+}$, this was shown to bind to copper-depleted AGAO but was unable to reoxidize $TPQ_{red}$ to $TPQ_{ox}$ (*31*). In contrast, in Zn-HPAO (*32*), Zn-LSAO (*28*), and Zn-ECAO (this study) TPQ reoxidation is observed. In addition, all three Zn-substituted CuAOs reacted with suicide inhibitors forming stable adducts, and Zn-LSAO was shown to be able to support the reductive half-reaction (*28*). However, none of the Zn-substituted CuAOs so far reported have been able to carry out the oxidative half-reaction, in contrast to the Co- and Ni-substituted enzymes which show low activity. These observations cannot be reconciled with either a purely redox-active or redox-inactive model for the CuAO active site metal. Therefore, we suggest that a distinction should be made between reoxidation of a chemically reduced cofactor and the oxidative half-cycle of catalytic turnover.

Dithionite-reduced TPQ is likely to be protonated at physiological pH and therefore unable to coordinate the metal. However, upon metal addition a rapid reoxidation of TPQ is observed, and the crystal structures of metal-substituted ECAOs show an on-metal TPQ binding, also indicative of oxidized TPQ (data not shown). It seems plausible that there is a site in the vicinity of the metal where dioxygen can bind and reoxidize TPQ. Copper and cobalt are able to directly bind oxygen (*59*, *63*). Nickel(II) complexes with dioxygen have been reported (*64*, *65*), but we have not found reference to zinc(II) dioxygen complexes. The ability of Zn-ECAO to support TPQ reoxidation suggests that, in this reaction, electrostatic stabilization of a dioxygen species rather than direct coordination is occurring (*36*). Once TPQ is oxidized, we suggest that in the Zn-substituted ECAO an on-metal conformation of TPQ is strongly favored as indicated by the UV−visible spectrum (*66*). However, it is clear that in the presence of excess 2-HP the on-metal/off-metal equilibrium is affected such that all of the TPQ becomes available for reaction with the inhibitor.

Our data, and that of others, show that in the Zn-enzyme the oxidative half-reaction is completely blocked. We therefore propose that reduced TPQ in metal-depleted ECAO can be oxidized by addition of metal in the presence of oxygen with no associated metal-redox change. This is analogous to the final step of TPQ biogenesis, $TPQ_{red} \rightarrow TPQ_{ox}$ (*67*). Once oxidized, TPQ is then competent for a single reductive half-reaction, but in the presence of Zn the resulting aminoquinol cannot be reoxidized to TPQ (Figure 7).

All metals were added to the Cu-free ECAO in their divalent state and, given the similarity of the coordination environment prior to addition of the metal, are unlikely to undergo subsequent oxidation state changes (*34*, *58*). The standard redox potentials for the transition metal ions studied suggest that only the Cu(II)/Cu(I) couple with $E_0$ +200 mV (*59*) would be thermodynamically capable to participate in oxidation of the aminoquinol cofactor during the oxidative half-cycle ($E_0$ for $TPQ_{ox}/TPQ_{red} = -140$ mV (*60*)). By contrast, as argued by Mills and Klinman (*32*), the much lower $E_0$ for Co(II)/Co(I) = −500 mV (*61*) suggests it would not be able to oxidize reduced TPQ while the Ni(II)/Ni(I) is even lower (−1160 mV (*62*)). Mills and Klinman argue against Co(III)/Co(II) redox mechanisms and propose an outer-sphere electron transfer role for the copper based on the fact that, despite compromised oxygen binding, the Co-HPAO can catalyze the enzymatic reaction (*32*). For ECAO, we have not determined the redox state of the Co but have no reason to doubt that it is likely to also be present as Co(II). While Co-ECAO does display catalytic potential, this is not restored to full activity in the presence of saturating oxygen and so does not behave in an identical manner to Co-HPAO (*32*). It is possible that the $K_{M(O_2)}$

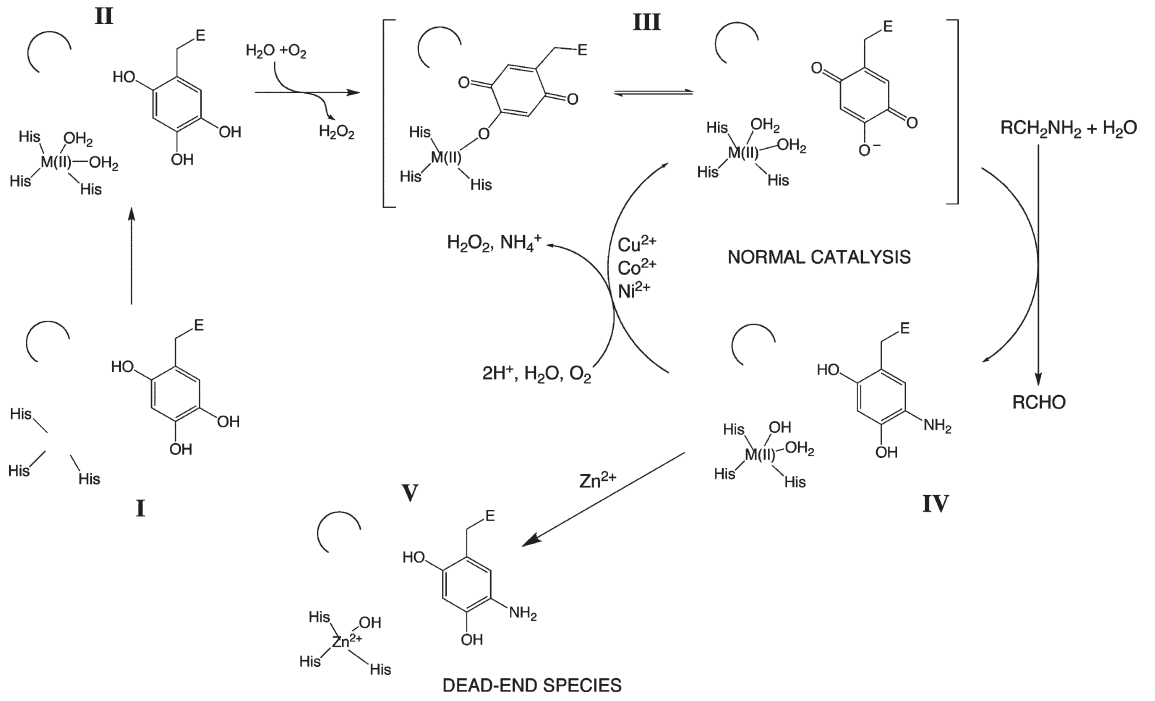


FIGURE 7: Mechanism proposed for the role of the active site metal in TPQ oxidation and catalysis. I represents the resting state of metal-free ECAO. II is metal- (M-) substituted ECAO in which the TPQ is fully reduced to the O-quinol. III is the oxidized form of TPQ which is in a metal-dependent rate-determining equilibrium between the unproductive "on-copper" and productive "off-copper" conformations. IV is the substrate-reduced TPQ aminoquinol which is able to form in the presence of all metals tested. V is the proposed $Zn^{2+}$-dead-end species. Unlike zinc, which is not competent to support reoxidation of the aminoquinol, the other metals tested (Cu, Co, and Ni) are able to support turnover.

for Co-ECAO may be substantially higher than that reported for Co-HPAO, but this would not be technically possible to determine.

Our data do not require a redox role for the metal as being essential for the oxidative half-cycle of ECAO; they are consistent with the redox step in the catalytic oxidative cycle involving direct electron transfer from reduced TPQ to dioxygen with the metal stabilizing the process. Cu is well suited to this role, Co less so, and Ni is poor with Zn unable to function. Alternatively, as copper has been shown to be the most favorable metal for supporting catalysis in ECAO, it could be argued that this is consistent with a redox role involving a Cu(I)-$TPQ_{SQ}$ intermediate in line with recent evidence for PSAO and AGAO (*38*, *39*). However, an outer-sphere electron transfer mechanism would still be required to explain the observed catalytic activity in Co-ECAO, Co-BSAO (*27*), and Co-HPAO (*32*). Shepard et al. suggested the possibility that an outer-sphere mechanism may operate for the Co- and Ni-substituted forms of AGAO (*30*).

*Peripheral Metal Sites*. The observation that addition of calcium to copper-reconstituted ECAO resulted in increased ECAO activity prompted us to investigate the peripheral metal binding sites more closely. The roles of these peripheral metals have not been examined previously. ECAO has a natural preference for calcium in these sites and so provides an excellent model for investigating the role of calcium sites in eukaryotic, and specifically mammalian, CuAOs. We were therefore interested to know whether these sites play any role in the function of the mature enzyme.

Upon treating wild-type ECAO with EDTA a reduction in enzyme activity of 60−90% was observed together with a lag phase (up to 4 min) before the enzyme acquired maximal activity. An investigation of the origin of this lag showed that it was not due to inadequate temperature control, interference by EDTA in the coupled assay, or EDTA acting as a reversible inhibitor. The addition of an excess of the metal ions $Ca^{2+}$, $Mg^{2+}$, $Mn^{2+}$, and $Sr^{2+}$ all allowed recovery of substantial enzyme activity and removed the lag observed after EDTA treatment alone. It should be noted that the only other report of a CuAO where the removal of a buried metal site and its effect upon activity has been measured is PSAO (*20*). In PSAO, EDTA treatment resulted in successful removal of the buried site $Mn^{2+}$, as confirmed by the absence of a characteristic paramagnetic Mn(II) EPR signal, but no effect on PSAO activity was observed. However, no data are available as to whether an EPR-silent divalent or a monovalent cation from the reaction buffer was able to occupy the vacated $Mn^{2+}$ site.

The X-ray structures of EDTA-treated enzyme revealed that buffer-derived sodium ions occupy both peripheral metal sites. In contrast to the untreated enzyme, in these structures TPQ exists in two conformations, the productive "off-copper" and the nonproductive "on-copper" conformers, each at 50% occupancy. The productive conformation of TPQ is that observed in previous structures (*19*, *21*, *23*, *25*, *40*, *44*, *68*) in which O4 is hydrogen-bonded to the hydroxyl group of Y369 (in ECAO) and O5 is positioned at the base of the amine substrate entry channel (Figure 1). In the nonproductive on-copper conformation TPQ has rotated about the Cα−Cβ bond so that O4 is close to the copper (*19*, *20*, *22*). Conformational rearrangement of TPQ from the on-copper to the active off-copper position may account for the lag phase observed upon enzyme assay of the EDTA-treated ECAO. Abolishment of the lag phase after addition of excess $Ca^{2+}$, $Mg^{2+}$, $Mn^{2+}$, or $Sr^{2+}$ suggests that binding of these metals in the peripheral binding sites may affect the TPQ conformation in the active site.

As we have clearly seen from the crystal structure of the EDTA-treated enzyme ($EDTA_1$), there is a direct effect of the identity of the peripheral sites ions on the conformation of the active site. The presence of 50% of the TPQ in the nonproductive on-copper conformation in the EDTA-treated

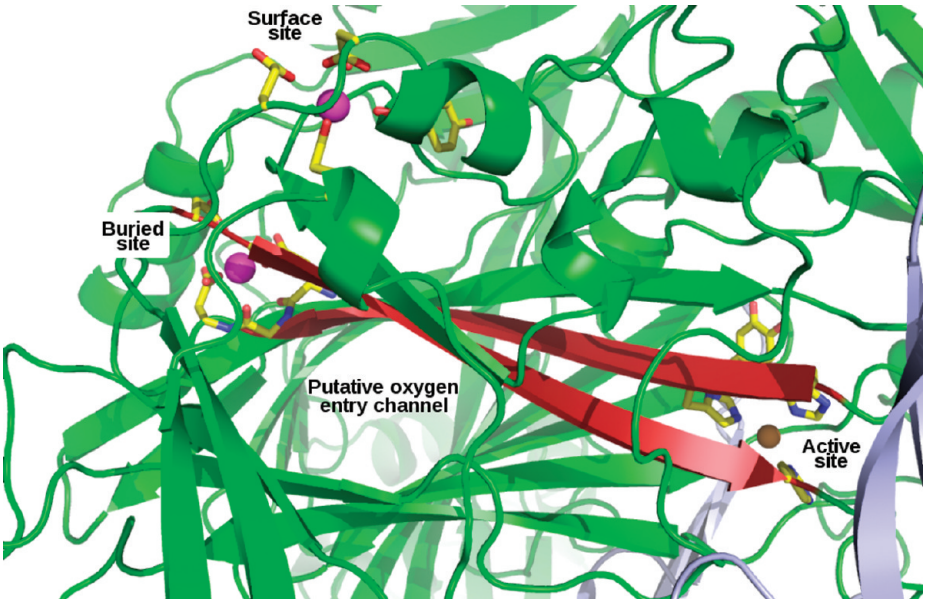


FIGURE 8: Structural relationship between the peripheral calcium sites and the active site in ECAO. The buried site is structurally associated with the active site (Cu and TPQ) through two $\beta$-strands (red). In contrast, the surface site shows no direct structural association with the active site. The putative oxygen entry channel is also shown.

structures suggests a long-range conformational effect is affecting TPQ mobility. Interestingly, in all amine oxidase structures determined, the buried metal and its ligands (or equivalent in HPAO) lie at one end of an antiparallel $\beta$-strand feature, the other end being occupied by two of the three His residues that coordinate the active site copper ion (Figures 2 and 8), providing a direct structural link between the two metals. However, whether this feature is responsible for influencing the mobility of TPQ cannot be established from the present crystallographic data because any small structural changes propagated through the enzyme are beyond the resolution limit of the data.

An alternative explanation for the reduced activity after EDTA treatment relates to the efficiency of oxygen entry to the active site. There have been several recent structural studies using xenon as a probe of potential molecular oxygen binding sites to explore potential pathways by which $O_2$ may be directed to the active site of CuAOs (*24*, *56*, *69*, *70*). These structures, together with *in silico* studies of HPAO, PSAO, AGAO, and PPLO (*70*), support a major pathway for oxygen entry from the surface through a conserved $\beta$-sandwich which links both metal sites to the active site copper (Figure 8) (*56*). In this $\beta$-sandwich many of the residues are conserved and form part of a funnel-shaped hydrophobic channel identified as the likely major oxygen entry pathway (*70*). Removal of the calcium ions from the peripheral metal sites may subtly alter the conformation or dynamics of the funnel-shaped channel, making the access of oxygen to the active site less efficient. We are currently investigating this possibility using biophysical and *in silico* methods. The observations that the lag phase is reduced and activity increases in the EDTA-treated enzyme when exposed to saturating oxygen conditions are of interest in this regard.

Whatever the cause of the reduced enzyme activity and lag, the removal of calcium from the peripheral metal sites of the enzyme causes a reduction in enzyme activity. However, removal of calcium does not completely abolish activity, indicating that calcium binding at these sites is not essential for activity. Even after calcium removal both sites are still occupied by a metal ion, generally a monovalent cation from the buffer. If the peripheral sites are reoccupied by a divalent cation ($Ca^{2+}$, $Mn^{2+}$, $Mg^{2+}$, $Sr^{2+}$), a substantial increase in activity is observed. As reported for other CuAOs, in ECAO it appears that the peripheral sites bind the most abundant solution metal ions with a strong preference for divalent cations. In the *E. coli* periplasm, as in mammalian systems, the most abundant divalent metal ion is calcium (*71*, *72*), and both solution studies and the structure of ECAO determined from crystals grown in ammonium sulfate show that calcium is the native ion occupying both peripheral metal binding sites (*19*). The next question is whether these peripheral metals play any role(s) at earlier stages in the enzyme production and processing pathway, and we are currently addressing this question by mutagenesis and kinetic, spectroscopic, and structural studies.

## CONCLUSIONS

We have undertaken initial studies to explore the replacement of the active site metal in ECAO. These data demonstrate that copper is the most efficient metal in supporting amine oxidation. Cobalt displays a low level of activity (ca. 4%) under air-saturated conditions, but unlike Co-HPAO, the turnover rate of Co-ECAO under oxygen saturating conditions only increases to 5.8% that of wild type and is not fully restored as observed for Co-HPAO. Nickel displays very low levels of activity (0.05%) while zinc is completely inactive. All of the metals support reoxidation of the dithionite-reduced TPQ cofactor and are able to react with 2-HP, including zinc, leading us to propose that this step is analogous to the final step in TPQ biogensis ($TPQ_{red}$ to $TPQ_{ox}$) and does not require a redox-active metal. Our data do not discriminate between the redox step in the catalytic oxidative half-reaction involving direct electron transfer from reduced TPQ to dioxygen with the metal stabilizing the process or with copper playing a direct redox role (Cu(I)-$TPQ_{SQ}$). In the latter case an alternative outer-sphere electron transfer mechanism would be required for the activity of the Co-ECAO. Surprisingly, we observed an effect of the peripheral calcium sites upon enzyme activity and undertook studies to investigate the role of these peripheral metals by their removal and replacement. Removing

the metals resulted in a 60−90% reduction in enzyme activity, and replacement with various divalent metals ($Ca^{2+}$, $Mn^{2+}$, $Mg^{2+}$, and $Sr^{2+}$) could restore full activity. We also observed that the surface site is readily exchangeable and is often occupied by sodium derived from *in vitro* buffers, meaning that it is difficult to prepare enzyme that lacks peripheral metals. Future studies to elucidate the roles of the individual peripheral sites by mutagenesis are underway.

## ACKNOWLEDGMENT

We thank Dr. Malcolm Halcrow and Dr. Mark Parsons for critical discussions.

## REFERENCES

1. Parrott, S., Jones, S., and Cooper, R. A. (1987) 2-Phenylethylamine catabolism by *Escherichia coli* K12. *J. Gen. Microbiol. 133*, 347–351.
2. Hacisalihoglu, A., Jongejan, J. A., and Duine, J. A. (1997) Distribution of amine oxidases and amine dehydrogenases in bacteria grown on primary amines and characterization of the amine oxidase from *Klebsiella oxytoca*. *Microbiology 143*, 505–512.
3. Knowles P. F., and Dooley D. M. (1994) Metalloenzymes involving amino acid-residue and related radicals, in Metal Ions in Biological Systems (Sigel H., and Sigel, A., Eds.) pp 361−403, Marcel Dekker, New York.
4. Moller, S., and McPherson, M. J. (1998) Developmental expression and biochemical analysis of the *Arabidopsis atao1* gene encoding an $H_2O_2$-generating diamine oxidase. *Plant J. 13*, 781–791.
5. Salmi, M., Hellman, J., and Jalkanen, S. (1998) The role of two distinct endothelial molecules, vascular adhesion protein-1 and peripheral lymph node addressin, in the binding of lymphocyte subsets to human lymph nodes. *J. Immunol. 160*, 5629–5636.
6. Elmore, B. O., Bollinger, J. A., and Dooley, D. M. (2002) Human kidney diamine oxidase: heterologous expression, purification, and characterization. *J. Biol. Inorg. Chem. 7*, 565–579.
7. Yu, P. H., Wright, S., Fan, E. H., Lun, Z. R., and Gubisne-Harberle, D. (2003) Physiological and pathological implications of semicarbazide-sensitive amine oxidase. *Biochim. Biophys. Acta 1647*, 193–199.
8. Wang, S. X., Mure, M., Medzihradszky, K., Burlingame, A., Brown, D. E., Dooley, D. M., Smith, A., Kagan, H. M., and Klinman, J. P. (1996) A crosslinked cofactor in lysyl oxidase: redox function for amino acid side chains. *Science 273*, 1078–1084.
9. Schwelberger, H. G. (2007) The origin of mammalian plasma amine oxidases. *J. Neural. Transm. 114*, 757–762.
10. Matyus, P., Dajka-Halasz, B., Foldi, A., Haider, F., Barlocco, D., and Magyar, K. (2004) Semicarbazide-sensitive amine oxidase: current status and perspectives. *Curr. Med. Chem. 11*, 1285–1298.
11. Gokturk, C., Nordquist, J., Sugimoto, H., Forsberg-Nilsson, K., Nilsson, J., and Oreland, L. (2004) Semicarbazide-sensitive amine oxidase in transgenic mice with diabetes. *Biochim. Biophys. Res. Commun. 325*, 1013–1020.
12. Smith, D. J., Salmi, M., Bono, P., Hellman, J., Leu, T., and Jalkanen, S. (1998) Cloning of vascular adhesion protein 1 reveals a novel multifunctional adhesion molecule. *J. Exp. Med. 188*, 17–27.
13. Salmi, M., Yegutkin, G. G., Lehvonen, R., Koskinen, K., Salminen, T., and Jalkanen, S. (2001) A cell surface amine oxidase directly controls lymphocyte migration. *Immunity 14*, 265–276.
14. Gubisne-Haberle, D., Hill, W., Kazachkov, M., Richardson, J. S., and Yu, P. H. (2004) Protein cross-linkage induced by formaldehyde derived from semicarbazide-sensitive amine oxidase-mediated deamination of methylamine. *J. Pharmacol. Exp. Ther. 310*, 1125–1132.
15. Moldes, M., Feve, B., and Pairault, J. (1999) Molecular cloning of a major mRNA species in murine 3T3 adipocyte lineage. differentiation-dependent expression, regulation, and identification as semicarbazide-sensitive amine oxidase. *J. Biol. Chem. 274*, 9515–9523.
16. Shepard, E. M., Smith, J., Elmore, B. O., Kuchar, J. A., Sayre, L. M., and Dooley, D. M. (2002) Towards the development of selective amine oxidase inhibitors. Mechanism-based inhibition of six copper containing amine oxidases. *Eur. J. Biochem. 269*, 3645–3658.
17. Janes, S. M., Mu, D., Wemmer, D., Smith, A. J., Kaur, S., Maltby, D., Burlingame, A. L., and Klinman, J. P. (1990) A new redox cofactor in eukaryotic enzymes: 6-hydroxydopa at the active site of bovine serum amine oxidase. *Science 248*, 981–987.
18. Dubois, J. L., and Klinman, J. P. (2005) Mechanism of post-translational quinone formation in copper amine oxidases and its relationship to the catalytic turnover. *Arch. Biochem. Biophys. 433*, 255–265.
19. Parsons, M. R., Convery, M. A., Wilmot, C. M., Yadav, K., Blakeley, V., Corner, A. S., Phillips, S. E. V., McPherson, M. J., and Knowles, P. F. (1995) Crystal structure of a quinoenzyme: copper amine oxidase of *Escherichia coli* at 2 Å resolution. *Structure 3*, 1171–1184.
20. Kumar, V., Dooley, D. M., Freeman, H. C., Guss, J. M., Harvey, I., McGuirl, M. A., Wilce, M. C. J., and Zubak, V. M. (1996) Crystal structure of a eukaryotic (pea seedling) copper-containing amine oxidase at 2.2 Å resolution. *Structure 4*, 943–955.
21. Wilce, M. C. J., Dooley, D. M., Freeman, H. C., Guss, J. M., Matsunami, H., McIntire, W. S., Ruggiero, C. E., Tanizawa, K., and Yamaguchi, H. (1997) Crystal structures of the copper-containing amine oxidase from *Arthrobacter globiformis* in the holo and apo forms: implications for the biogenesis of topaquinone. *Biochemistry 36*, 16116–16133.
22. Li, R. B., Klinman, J. P., and Mathews, F. S. (1998) Copper amine oxidase from *Hansenula polymorpha*: the crystal structure determined at 2.4 Å resolution reveals the active conformation. *Structure 6*, 293–307.
23. Duff, A. P., Cohen, A. E., Ellis, P. J., Kuchar, J. A., Langley, D. B., Shepard, E. M., Dooley, D. M., Freeman, H. C., and Guss, J. M. (2003) The crystal structure of *Pichia pastoris* lysyl oxidase. *Biochemistry 42*, 15148–15157.
24. Lunelli, M., Di Paolo, M. L., Biadene, M., Calderone, V., Battistutta, R., Scarpa, M., Rigo, A., and Zanotti, G. (2005) Crystal structure of amine oxidase from bovine serum. *J. Mol. Biol. 346*, 991–1004.
25. Airenne, T. T., Nymalm, Y., Kidron, H., Smith, D. J., Pihlavisto, M., Salmi, M., Jalkanen, S., Johnson, M. S., and Salminen, T. A. (2005) Crystal structure of the human vascular adhesion protein-1: unique structural features with functional implications. *Protein Sci. 14*, 1964–1974.
26. McGrath, A. P., Hilmer, K. M., Collyer, C. A., Shepard, E. M., Elmore, B. O., Brown, D. E., Dooley, D. M., and Guss, J. M. (2009) Structure and inhibition of human diamine oxidase. *Biochemistry 48*, 9810–9822.
27. Suzuki, S., Takeshi, S., Nakahara, A., Oda, O., Manabe, T., and Okuyama, T. (1981) Preparation and characterization of cobalt(II)-substituted bovine serum amine oxidase. *J. Biochem. 90*, 905–908.
28. Padiglia, A., Medda, R., Pedersen, J. Z., Agrò, A. F., Lorrai, A., Murgia, B., and Floris, G. (1999) Effect of metal substitution in copper amine oxidase from lentil seedlings. *J. Biol. Inorg. Chem. 4*, 608–613.
29. Mura, A., Padiglia, A., Medda, R., Pintus, F., Agro, A. F., and Floris, G. (2006) Properties of copper-free pig kidney amine oxidase: role of topa quinine. *FEBS Lett. 580*, 4317–4324.
30. Padiglia, A., Medda, R., Bellelli, A., Agostinelli, E., Morpurgo, L., Mondovi, B., Agro, A. F., and Floris, G. (2001) The reductive and oxidative half-reactions and the role of copper ions in plant and mammalian copper-amine oxidases. *Eur. J. Inorg. Chem.* 35–42.
31. Kishishita, S., Okajima, T., Kim, M., Yamaguchi, H., Hirota, S., Suzuki, S., Kuroda, S., Tanizawa, K., and Mure, M. (2003) Role of copper ion in bacterial copper amine oxidase: spectroscopic and crystallographic studies of metal-substituted enzymes. *J. Am. Chem. Soc. 125*, 1041–1055.
32. Mills, S. A., and Klinman, J. P. (2000) Evidence against reduction of $Cu^{2+}$ to $Cu^{+}$ during dioxygen activation in a copper amine oxidase from yeast. *J. Am. Chem. Soc. 122*, 9897–9904.
33. Dooley, D. M., McGuirl, M. A., Brown, D. E., Turowski, P. N., McIntire, W. S., and Knowles, P. F. (1991) A Cu(I)-semiquinone state in substrate-reduced amine oxidases. *Nature 349*, 262–264.
34. Mills, S. A., Goto, Y., Su, Q., Plastino, J., and Klinman, J. P. (2002) Mechanistic comparison of the cobalt-substituted and wild-type copper amine oxidase from *Hansenula polymorpha*. *Biochemistry 41*, 10577–10584.
35. Agostinelli, E., Morpurgo, L., Wang, C., Giartosio, A., and Mondovi, B. (1994) Properties of cobalt-substituted bovine serum amine oxidase. *Eur. J. Biochem. 222*, 727–732.
36. Prabhakara, R., Siegbahn, P. E. M., and Minaev, B. F. (2003) A theoretical study of the dioxygen activation by glucose oxidase and copper amine oxidase. *Biochim. Biophys. Acta 1647*, 173–178.
37. Prabhakar, R., and Siegbahn, P. E. M. (2003) Theoretical study of the mechanism for the oxidative half-reaction of copper amine oxidase (CAO). *J. Phys. Chem. B 107*, 3944–3953.
38. Mukherjee, A., Smirnov, V. V., Lanci, M. P., Brown, D. E., Shepard, E. M., Dooley, D. M., and Roth, J. P. (2008) Inner-sphere mechanism for molecular oxygen reduction catalyzed by copper amine oxidases. *J. Am. Chem. Soc. 130*, 9459–9473.
39. Shepard, E. M., Okonski, K. M., and Dooley, D. M. (2008) Kinetics and spectroscopic evidence that the Cu(I)-semiquinone intermediate reduces molecular oxygen in the oxidative half-reaction of *Arthrobacter globiformis* amine oxidase. *Biochemistry 47*, 13907–13920.

40. Murray, J. M., Saysell, C. G., Wilmot, C. M., Tambyrajah, W. S., Jaeger, J., Knowles, P. F., Phillips, S. E., and McPherson, M. J. (1999) The active site base controls cofactor reactivity in *Escherichia coli* amine oxidase: X-ray crystallographic studies with mutational variants. *Biochemistry 38*, 8217–8227.
41. Crabbe, M. J., Waight, R. D., Bardsley, W. G., Barker, R. W., Kelly, I. D., and Knowles, P. F. (1976) Human placental diamine oxidase: improved purification and characterization of a copper- and manganese-containing amine oxidase with novel substrate specificity. *Biochem. J. 155*, 679–687.
42. Sebela, M., Luhova, L., Frebort, I., Hirota, S., Faulhammer, H. G., Stuzka, V., and Pec, P. (1997) Confirmation of the presence of a Cu(II)/topa quinone active site in the amine oxidase from fenugreek seedlings. *J. Exp. Bot. 48*, 1897–1907.
43. Murray, J. M., Kurtis, C. R., Tambyrajah, W. S., Saysell, C. G., Wilmot, C. M., Parsons, M. R., Phillips, S. E., Knowles, P. F., and McPherson, M. J. (2001) Conserved tyrosine-369 in the active site of *Escherichia coli* copper amine oxidase is not essential. *Biochemistry 40*, 12808–12818.
44. Saysell, C. G., Murray, J. M., Wilmot, C. M., Brown, D. E., Dooley, D. M., Phillips, S. E. V., McPherson, M. J., and Knowles, P. F. (2000) Investigation into the mechanism of $\lambda$max shifts and their dependence on pH for the 2-hydrazinopyridine derivatives of two copper amine oxidases. *J. Mol. Catal. B: Enzym. 8*, 17–25.
45. Mure, M., Brown, D. E., Saysell, C., Rogers, M. S., Wilmot, C. M., Kurtis, C. R., McPherson, M. J., Phillips, S. E. V., Knowles, P. F., and Dooley, D. M. (2005) Role of the interactions between the active site base and the substrate Schiff base in amine oxidase catalysis. Evidence from structural and spectroscopic studies of the 2-hydrazinopyridine adduct of *Escherichia coli* amine oxidase. *Biochemistry 44*, 1568–1582.
46. Leslie, A. G. W. (1992) *Joint CCP4 + ESF-EAMCB Newsletter on Protein Crystallography*, No. 26.
47. Evans, P. (1993) *Proceedings of the CCP4 Study Weekend*, 114−122.
48. Collaborative Computational Project, Number 4 (1994) Acta Crystallogr. *D50*, 760−763.
49. Murshudov, G. N., Vagin, A. A., and Dodson, E. J. (1997) Refinement of macromolecular structures by the maximum-likelihood method. *Acta Crystallogr. D53*, 240–255.
50. Emsley, P., and Cowtan, K. (2004) Coot: model-building tools for molecular graphics. *Acta Crystallogr. D60*, 2126–2132.
51. Furia, T. E. (1972) Sequestrants in food, in CRC Handbook of Food Additives (Furia, T. E., Ed.) Vol. *1*, 2nd ed., pp 271−294, CRC Press, Boca Raton, FL.
52. De Vries, S., Van Spanning, R. J. M., and Steinebach, V. (2000) A spectroscopic and kinetic study of *Escherichia coli* amine oxidase. *J. Mol. Catal. B: Enzym. 8*, 111–120.
53. Su, Q. J., and Klinman, J. P. (1998) Probing the mechanism of proton coupled electron transfer to dioxygen: the oxidative half-reaction of bovine serum amine oxidase. *Biochemistry 37*, 12513–12525.
54. Plastino, J., Green, E. L., Sanders-Loehr, J., and Klinman, J. P. (1999) An unexpected role for the active site base in cofactor orientation and flexibility in the copper amine oxidase from *Hansenula polymorpha*. *Biochemistry 38*, 8204–8216.
55. Mure, M., Mills, S. A., and Klinman, J. P. (2002) Catalytic mechanism of the topa quinone containing copper amine oxidases. *Biochemistry 41*, 9269–9278.
56. Pirrat, P., Smith, M. A., Pearson, A. R., McPherson, M. J., and Phillips, S. E. V. (2008) Structure of a xenon derivative of *Escherichia coli* copper amine oxidase: confirmation of the proposed oxygen-entry pathway. *Acta Crystallogr. F64*, 1105–1109.
57. Mure, M., and Klinman, J. P. (1993) Synthesis and spectroscopic characterization of model compounds for the active site cofactor in copper amine oxidases. *J. Am. Chem. Soc. 115*, 7117–7127.
58. Samuels, N. M., and Klinman, J. P. (2005) 2,4,5-Trihydroxyphenylalanine quinone biogenesis in the copper amine oxidase from *Hansenula polymorpha* with the alternate metal nickel. *Biochemistry 44*, 14308–14317.
59. Whittaker, J. W. (1999) Oxygen reactions of the copper oxidases. *Essays Biochem. 34*, 155–172.
60. Contakes, S. M., Juda, G. A., Langley, D. B., Halpern-Manners, N. W., Duff, A. P., Dunn, A. R., Gray, H. B., Dooley, D. M., Guss, J. M., and Freeman, H. C. (2005) Reversible inhibition of copper amine oxidase activity by channel-blocking ruthenium(II) and rhenium(I) molecular wires. *Proc. Natl. Acad. Sci. U.S.A. 102*, 13451–13456.
61. Drummond, J. T., and Matthews, R. G. (1994) Nitrous oxide degradation by cobalamin-dependent methionine synthase: characterization of the reactants and products in the inactivation reaction. *Biochemistry 33*, 3732–3741.
62. Gomes, L., Pereira, E., and de Castro, B. (2000) Nickel(II) complexes with $N_2OS$ and $N_2S_2$ co-ordination spheres: reduction and spectroscopic study of the corresponding Ni(I) complexes. *J. Chem. Soc., Dalton Trans. 8*, 1373–1379.
63. Lanci, M. P., Smirnov, V. V., Cramer, C. J., Gauchenova, E. V., Sundermeyer, J., and Roth, J. P. (2007) Isotopic probing of molecular oxygen activation at copper(I) sites. *J. Am. Chem. Soc. 129*, 14697–14709.
64. Cheng, C.-C., Gulia, J., Rokita, S. E., and Burrows, C. J. (1996) Dioxygen chemistry of nickel(II) dioxopentaazamacrocyclic complexes: substituent and medium effects. *J. Mol. Catal. A: Chem. 113*, 379–391.
65. Chen, D., Motekaitis, R. J., and Martell, A. E. (1991) Dioxygen adducts of nickel(II) and cobalt(II) dioxopentaazamacrocyclic complexes—kinetics, stabilities and hydroxylation of the ligands in the nickel dioxygen complexes. *Inorg. Chem. 30*, 1396–1402.
66. Foster, C. L., Liu, X. M., Kilner, C. A., Thornton-Pett, M., and Halcrow, M. A. (2000) Complexes of 2-hydroxy-5-methyl-1,4-benzoquinone as models for the "TPQ-on" form of copper amine oxidases. *J. Chem. Soc., Dalton Trans. 24*, 4563–4568.
67. Kim, M., Okajima, T., Kishishita, S., Yoshimura, M., Kawamori, A., Tanizawa, K., and Yamaguchi, H. (2002) X-ray snapshots of quinone cofactor biogenesis in bacterial copper amine oxidase. *Nat. Struct. Biol. 9*, 591–596.
68. Dawkes, H. C., and Phillips, S. E. V. (2001) Copper amine oxidase: cunning cofactor and controversial copper. *Curr. Opin. Struct. Biol. 11*, 666–673.
69. Duff, A. P., Trambaiolo, D. M., Cohen, A. E., Ellis, P. J., Juda, G. A., Shepard, E. M., Langley, D. B., Dooley, D. M., Freeman, H. C., and Guss, J. M. (2004) Using xenon as a probe for dioxygen-binding sites in copper amine oxidases. *J. Mol. Biol. 344*, 599–607.
70. Johnson, B. J., Cohen, J., Welford, R. W., Pearson, A. R., Schulten, K., Klinman, J. P., and Wilmot, C. M. (2007) Exploring molecular oxygen pathways in *Hansenula polymorpha* copper-containing amine oxidase. *J. Biol. Chem. 282*, 17767–17776.
71. Rosen, B. P. (1987) Bacterial calcium transport. *Biochim. Biophys. Acta 906*, 101–110.
72. Dominguez, D. C. (2004) Calcium signalling in bacteria. *Mol. Microbiol. 54*, 291–297.
73. http://www.delanoscientific.com.
74. Larkin, M. A., Blackshields, G., Brown, N. P., Chenna, R., McGettigan, P. A., McWilliam, H., Valentin, F., Wallace, I. M., Wilm, A., Lopez, R., Thompson, J. D., Gibson, T. J., and Higgins, D. G. (2007) Clustal W and Clustal X version 2.0. *Bioinformatics 23*, 2947–2948.